

BABEŞ-BOLYAI UNIVERSITY  
FACULTY OF PHYSICS

COMPUTER SIMULATION STUDY OF  
ENTANGLED MATERIALS

By

Ferenc Járαι-Szabó

A DISSERTATION

Submitted to the Faculty of Physics  
of the Babeş-Bolyai University  
in fulfillment of the requirements for  
the degree of Master of Computational Physics

**Scientific advisers:**

Prof. dr. David Rodney\* and Prof. dr. Rémi Dendievel\*

\* Institut National Polytechnique de Grenoble, Génie Physique et Mécanique des  
Matériaux, France

Cluj-Napoca, Romania  
2003

Ferenc Járαι-Szabó

# COMPUTER SIMULATION STUDY OF ENTANGLED MATERIALS

## **Abstract**

In this work a three-dimensional discrete version of the worm-like Kratky-Porod model for computer simulation of non-bonded entangled materials is proposed. The main ingredients of this model are hard-core (non-penetrable) and flexible fibers. Three main mechanisms govern the evolution of the system. The flexibility of fibers is considered through stretching of the discrete elements and the angle between neighboring ones. Non-penetrability is ensured by a repulsive potential between non-consecutive elements. Different mechanical properties are calculated for different compression processes in two different regimes: small and large deformation regime of the fibers. Energetic aspects of compression processes are studied, too.

# Contents

<b>1</b>	<b>Introduction</b>	<b>4</b>
<b>2</b>	<b>Computational model</b>	<b>6</b>
2.1	Energy model . . . . .	6
2.2	Quasi-static algorithm and compression . . . . .	8
2.3	Calculation of pressure and connectivity . . . . .	9
2.4	Typical numbers . . . . .	12
<b>3</b>	<b>Single fiber properties</b>	<b>13</b>
3.1	Small deformation regime . . . . .	13
3.2	Large deformation regime . . . . .	15
<b>4</b>	<b>Small deformation of component fibers</b>	<b>16</b>
4.1	Relaxation method . . . . .	16
4.2	Compression method . . . . .	17
<b>5</b>	<b>Large deformations of component fibers</b>	<b>21</b>
5.1	Evolution curves . . . . .	21
5.2	Finite size effects . . . . .	22
<b>6</b>	<b>Conclusions and perspectives</b>	<b>25</b>

# List of Figures

2.1	A sketch about the modeled fibers in interaction. The notations of this figure will be used in the rest of this work. . . . .	7
2.2	An initial unrelaxed tangle generated with a random walk algorithm.	9
2.3	The image of a relaxed tangle with fibers shorter than the size of the simulation cell obtained from the above presented initial system. . . .	10
2.4	A snapshot of the compressed tangle. . . . .	11
3.1	The outline of the bending test. . . . .	14
3.2	The scaled results for small deformation regime including the analytic formula (full line), too. . . . .	14
3.3	Bending-test results for large deformations of single fibers. . . . .	15
4.1	Evolution-curves for the connectivity at small deformations obtained with the relaxation method. . . . .	17
4.2	Evolution curves for pressure at small deformation of component fibers.	18
4.3	The dependence of the threshold volume-fraction on the aspect ratio of fibers. . . . .	18
4.4	Evolution curves for the number of links per fiber, obtained with the compression method for different bending stiffnesses. . . . .	19
4.5	Evolution of pressure, obtained with the compression method for different bending stiffnesses. . . . .	20
4.6	Energetic aspects for a compression process of a tangle with length $L = 4$ of component fibers. . . . .	20
5.1	The simulation curves obtained for the compression in high deformation regime for the evolution of connectivity. . . . .	22
5.2	The simulation curves obtained for the compression in high deformation regime for the evolution of the pressure. . . . .	23

5.3 The evolution curves of different energy types for compression of a tangle in high deformation regime. . . . . 23

5.4 The underestimation of links caused by imposed boundary conditions. 24

5.5 Evolution curves showing no influence of boundaries on the pressure. 24

# 1

## Introduction

Entangled materials are abundant and of very different origins and usage. They are at the heart of living cells (cytoskeletal polymers) [7], of two dimensional non-woven textile fabrics and papers [5], of glass-wool [3] and more generally of polymer melts. Three-dimensional entangled networks are also found in the technologically attractive composite fiber reinforced polymers which are potential candidates for optimized mechanical [10] and electrical properties [4].

Little is known about the connection between the macroscopic collective properties of tangles and underlying microscopic properties of component fibers and of their mutual interactions.

Mechanical behaviors have been studied experimentally by means, for example constant strain rate compressions in the case of glass-wool [3] and shearing tests in the case of living cells [12]. Electrical conductivity has also been considered [9]. These experiments show a percolation transition both in rigidity and conductivity, followed by non-linear behaviors.

On the computational side, two types of simulation have mainly been performed. On the one hand, percolation was studied in rigid, soft-core (penetrable) rod systems [1, 2]. On the other hand, simulations of mechanical properties focused on two-dimensional bonded media, representative of textile fabrics [5] are known. The rupture process of disordered materials pulled by a uniaxial force is simulated using  $(1 + 1)$  dimensional fiber bundle models [6]. This type of model can be also applied to study the evolution of mechanical properties of an entangled media through different type of processes.

We propose a three-dimensional discrete version of the worm-like Kratky-Porod

model [8] accounting for the bending and stretching properties of fibers. The interactions between them ensuring their non-penetrability is taken into account via a repulsive potential centered at the nodes used to discretize the fibers. This model is applied to study non-bonded (no fixed cross-link) tangles and we consider different micro- and macroscopic mechanical properties through a compression process for small and large deformation regimes. A connectivity transition is detected at small deformations which should be linked to the electrical conductivity of tangles.

We try to understand how flexible polymers build up statistical networks, which types of deformation have the dominant contribution to the network elasticity and what kind of effective description of the complicated microscopic network geometry should be used.

In the next chapter the computational model is presented which is followed by a study of the mechanical properties (stretching and bending) of single fibers in the small and the large deformation regime. The fourth chapter contains our results concerning the entanglement transition observed at low fiber densities. In the fifth chapter is presented the evolution of the mechanical properties of a tangle in the high deformation regime. In the last chapter our conclusions obtained from the presented simulations are summarized.

## 2

# Computational model

This model is used to study mechanical properties of tangles composed of non-bonded, flexible, non-penetrable long fibers with the same initial lengths. Is a three-dimensional discrete version of the worm-like Kratky-Porod model [8] inspired from the methods developed for atomic scale simulations of polymers, applied for long fibers [11].

Fig. 2.1 is a sketch showing two fibers in interaction containing the used notations too. Fibers are built up with series of straight tensile segments of length  $l_i$  (the  $l_0$  initial length is the same for all), with different angles  $\theta_i$  between neighboring ones. The discretization points between adjoining segments are called "nodes". Their positions are the degrees of freedom of our model. For each node is known the position vector and its neighboring nodes. In this way a component fiber can be characterized by  $n_{nodes}$  node-points. The number of fibers in a tangle is  $N_{fiber}$ .

For simulation field an  $A_0$  sized cube is used which implies the applied restricted boundary conditions. The fibers can move only inside, in the volume of this simulation cell.

## 2.1 Energy model

Three types of main mechanisms govern the evolution of the system. The first contribution is the stretching of the segments which is modeled with a spring-potential for each segment:

$$E_S^{(i)} = \frac{1}{2}k_S \left( \frac{l_i - l_0}{l_0} \right)^2 . \quad (2.1)$$

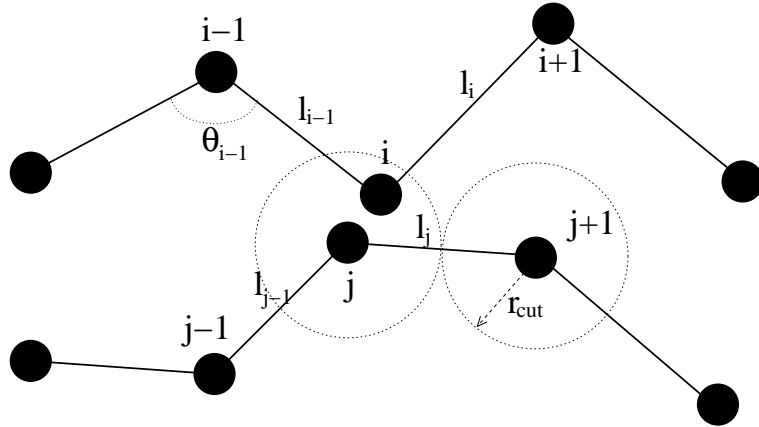


Figure 2.1: A sketch about the modeled fibers in interaction. The notations of this figure will be used in the rest of this work.

The second contribution is the bending of the fibers modeled with an angular-potential depending on the angle between consecutive segments:

$$E_B^{(i)} = \frac{1}{2} k_B (\theta_i - \pi)^2, \quad (2.2)$$

adapted from molecular models of polymers with covalent angle of  $\pi$ . This first two terms ensure that in absence of interactions between fibers the equilibrium shape for a fiber is a straight line of length  $(n_{nodes} - 1)l_0$ .

The third term is the repulsive interaction potential between non-consecutive nodes. This term ensures an excluded volume around the fibers and avoids crossing of the fibers. The potential used is:

$$E_I^{(ij)} = -k_I \ln \left( \frac{r_{ij}}{r_{cut}} \right) e^{\frac{r_{ij}}{r_{cut}}}, \quad (2.3)$$

where the exponential term ensures a smooth vanishing of the potential at the cut-off radius  $r_{cut}$ . With this exponential correction term the calculations may have a precision limit, which impose the use of an effective radius defined by the equation

$$F_I(r_{eff}) = F_{min}, \quad (2.4)$$

where  $F_{min}$  is the minimum detectable force within the precision limit of calculations (in our case  $r_{eff} = 0.92 r_{cut}$ ).

From this point of view of the effective interaction radius, fibers are composed by  $n_{nodes}$  of spheres of  $r_{eff}$  radius. The ratio between the volume of this spheres and the total volume of the simulation cell defines the volume-fraction

$$V_f = \frac{V_{fibers}}{V_0} = \frac{4\pi}{3} \frac{r_{eff}^3}{V_0} n_{nodes} N_{fibers}, \quad (2.5)$$

which is a dimensionless characteristic quantity for tangles. The other dimensionless characteristic quantity is the aspect ratio of the fibers defined as  $\frac{L}{r_{eff}}$ .

The bending, stretching and interaction stiffnesses ( $k_B, k_S, k_I$ ) can be chosen independently and they govern directly the microscopical rules in the tangle.

## 2.2 Quasi-static algorithm and compression

The different potentials are used to calculate the forces on each node by taking its gradients. In this way on the  $i$ th node three types of forces can be calculated:

$$\mathbf{F}_S^{(i)} = -k_S \frac{l_{i-1} - l_0}{l_0^2} \mathbf{t}_{i-1} + k_S \frac{l_i - l_0}{l_0^2} \mathbf{t}_i \quad (2.6)$$

$$\mathbf{F}_B^{(i)} = k_B (\theta_{i-1} - \pi) \mathbf{t}_{i-1}^\perp + k_B (\theta_{i+1} - \pi) \mathbf{t}_i^\perp - k_B (\theta_i - \pi) (\mathbf{t}_{i-1}^\perp - \mathbf{t}_i^\perp) \quad (2.7)$$

$$\mathbf{F}_I^{(ij)} = -\frac{k_I}{r_{cut}} e^{\frac{r_{ij}}{r_{ij} + r_{cut}}} \left( \frac{r_{cut}}{r_{ij}} - \ln \frac{r_{ij}}{r_{ij} + r_{cut}} \right) \mathbf{t}_{ij}, \quad (2.8)$$

where  $\mathbf{t}_i$  is a unit vector in the direction of the  $i$ th segment pointing from the  $(i-1)$ th node to  $i$ th node,  $\mathbf{t}_i^\perp$  is a perpendicular unit vector at the  $i$ th segment and  $\mathbf{t}_{ij}$  is a unit vector pointing from the  $i$ th node to the  $j$ th one.

Nodes are displaced step by step using over-dumped dynamics (first order Euler integration algorithm). The displacement of the  $i$ th node at each step is proportional to the sum of forces applied on it:

$$\Delta \mathbf{r}_i = \eta (\mathbf{F}_S + \mathbf{F}_B + \mathbf{F}_I), \quad (2.9)$$

where  $\eta$  is a fixed numerical viscosity factor.

Fig. 2.2 presents an initial configuration generated by a random walk algorithm which produces a tangle with randomly distributed, non stretched fibers with random segments-orientation.

A long initial relaxation ( $10^5$  steps) allows us to obtain an equilibrium configuration presented in the fig. 2.3. Compressions may then be applied by displacing all boundaries inward step by step relaxing the configuration between each step ( $3 \times 10^4$  steps). A compressed tangle can be seen in the fig. 2.4. In this figure the volume-fraction of the tangle is reduced by compression to half of its initial value. If the total displacement of one boundary is  $\Delta A$  and the initial length of the simulation cell is  $A_0$  then the new volume of the compressed cell will be

$$V = (A_0 - 2\Delta A)^3 = V_0(1 - \varepsilon)^3, \quad (2.10)$$

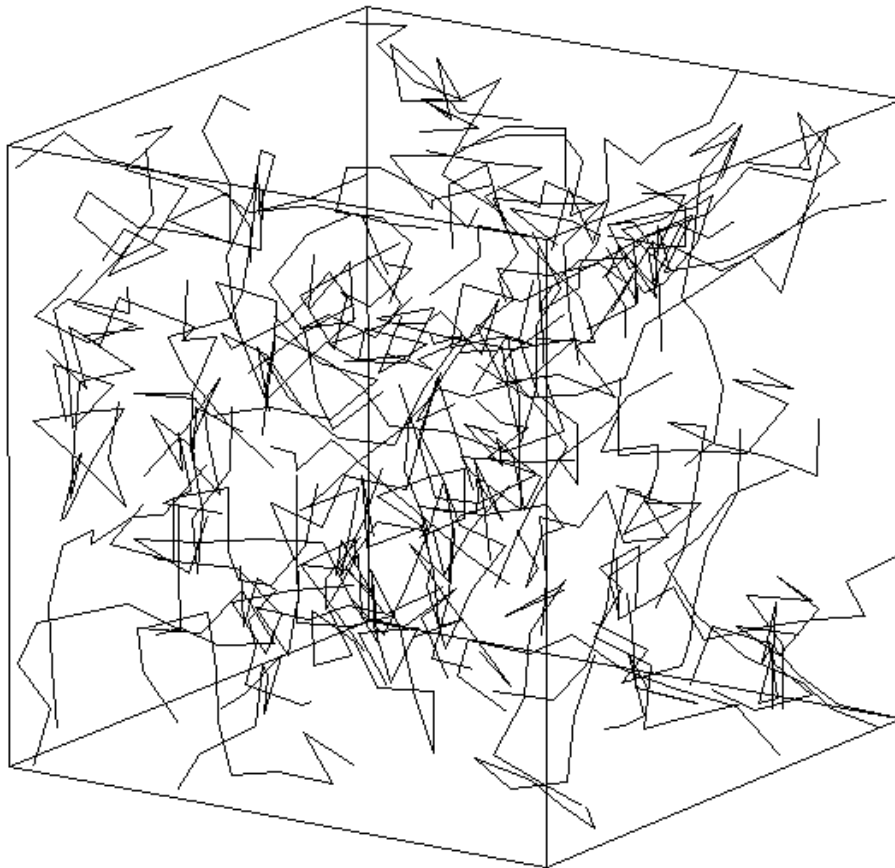


Figure 2.2: An initial unrelaxed tangle generated with a random walk algorithm.

where  $\varepsilon = \frac{2\Delta A}{A_0}$  is the total compression of the tangle. In this way the actual compression of the entangled media can be included in the (2.5) expression of the volume-fraction

$$V_f = \frac{4\pi}{3} \frac{r_{eff}^3}{V_0} \frac{1}{(1-\varepsilon)^3} n_{nodes} N_{fiber}. \quad (2.11)$$

The above-defined volume-fraction will be a universal dimensionless characteristic quantity used to describe the space filling of different tangles with different compressions.

## 2.3 Calculation of pressure and connectivity

Connectivity and pressure characterize the evolution of the tangle. They are the studied properties of the system, which can be linked to different mechanical and

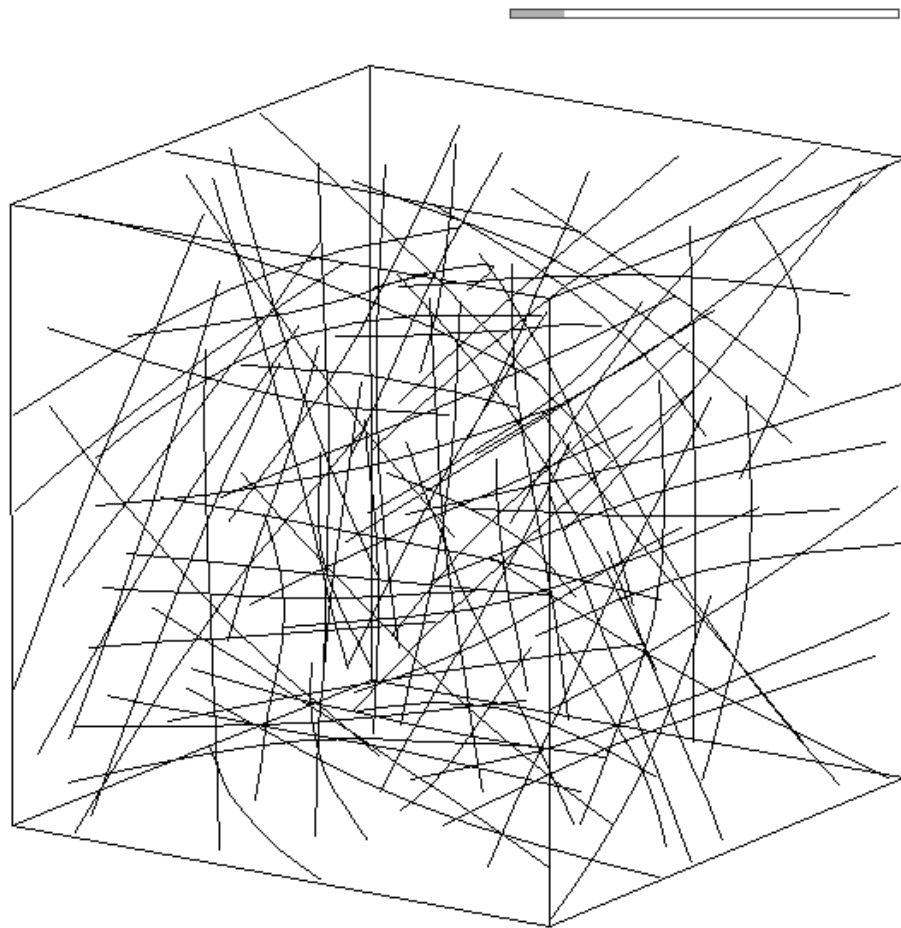


Figure 2.3: The image of a relaxed tangle with fibers shorter than the size of the simulation cell obtained from the above presented initial system.

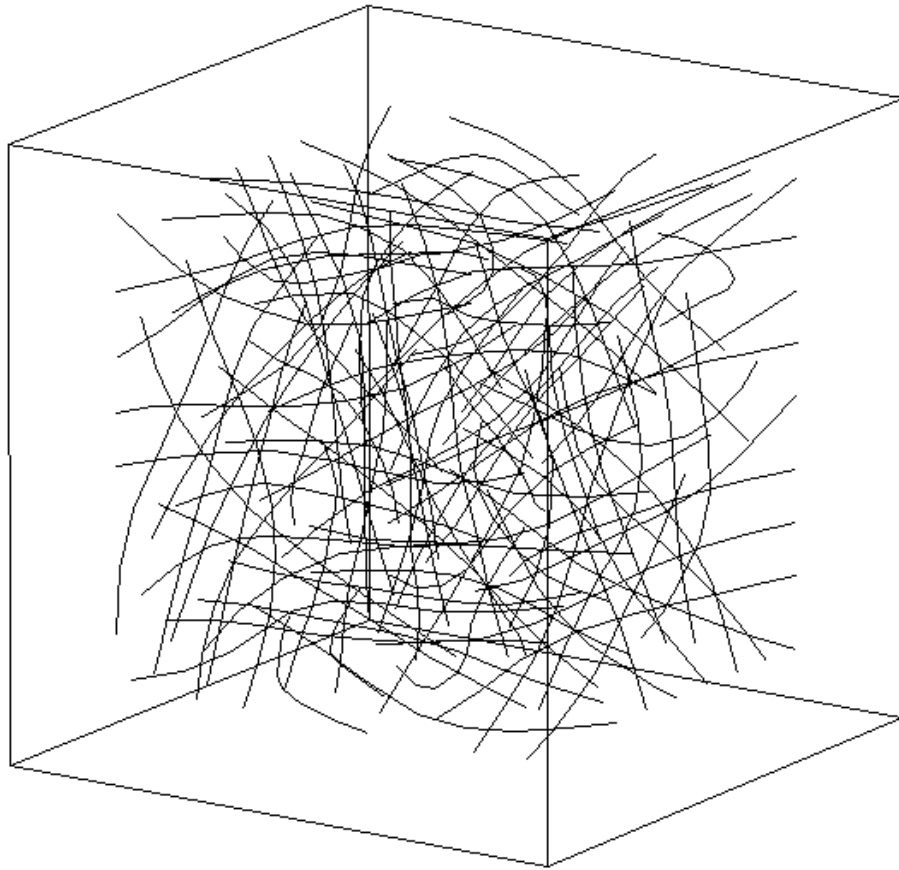


Figure 2.4: A snapshot of the compressed tangle.

electrical characteristics of entangled materials.

The pressure exerted by the tangle to a boundary is equal with the external force to be applied on this boundary to keep it in equilibrium, divided by its area. In equilibrium state it is also equal with opposite sign of the sum of internal forces perpendicular to the studied boundary on the nodes in contact with this, divided with the corresponding area. In an equilibrium system the pressures on different boundaries are equal which implies the use of the average value of them.

A link is defined as two non-consecutive nodes that are closer than the effective interaction radius. Links are computed taking care of counting only once if a node has contact with two consecutive nodes of other fibers. In this way the number of links between fibers can be calculated. The connectivity means the average number of links per fiber. This quantity is linked to the macroscopic mechanical and electrical properties of tangles and to the three-dimensional percolation phenomena, too.

## 2.4 Typical numbers

As simulation field an  $A_0 = 5$  sized box is used. The tangle is composed of fibers with  $L = 1 \div 5$  initial length and  $r_{cut} = 0.25$  ( $r_{eff} = 0.23$ ) cut-off radius.

In the relaxation process the  $\eta$  viscosity factor has an important role. This parameter has to be chosen taking care of magnitude of occurred forces. In the presented simulations this parameter was chosen to be  $\eta = 0.01$ .

In compressions the simulation cell is compressed to half of its initial volume, which means the doubling of the volume-fraction of an uncompressed tangle. Inward displacement of the boundaries through one compression step is  $\delta A = 0.02$ .

# 3

## Single fiber properties

First of all mechanical behaviors of single fibers have been studied. These fibers are the microscopic main ingredients of the present model. To model entangled media, flexible fibers were chosen but is also important to know how they behave when a force is applied on them.

Our choice of the stretching energy ensures the classical Hookian behavior. If  $F_S$  is the applied stretching force then the elongation of the fiber will be

$$\Delta L = \frac{F}{k_S^f}, \quad (3.1)$$

where  $k_S^f = \frac{k_I}{n_{nodes}-1}$  is the stretching stiffness of one fiber composed of  $(n_{nodes} - 1)$  segments.

To look at flexibility properties bending tests were performed which principle is presented in fig. 3.1. This tests are analogous with classical continuum mechanics tests [13]. The first two nodes of the fiber are fixed in order to impose clamped boundary condition. A vertical force is applied at the opposite end of the fiber, and the vertical displacement  $\Delta z$  is calculated at equilibrium. The simulation results are compared with known behavior of bended rods in the small and large deformation limits.

### 3.1 Small deformation regime

For small deformation regime stretching of segments is negligible. The potential energy contains only angular terms. Then it can be easily shown that the  $i$ th angle is  $(\pi - i\frac{Fl_0}{k_B})$ . In this approximation the vertical displacement is

$$\frac{\Delta z}{l_0} = \frac{Fl_0}{k_B} \left(\frac{L}{l_0}\right)^3 \frac{1}{3} \left(1 - \frac{l_0}{L}\right) \left(1 - \frac{1}{2} \frac{l_0}{L}\right). \quad (3.2)$$

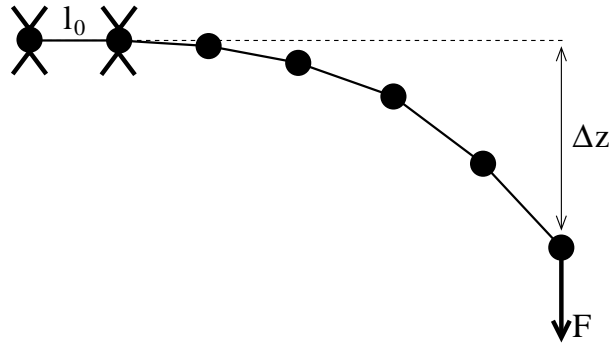


Figure 3.1: The outline of the bending test.

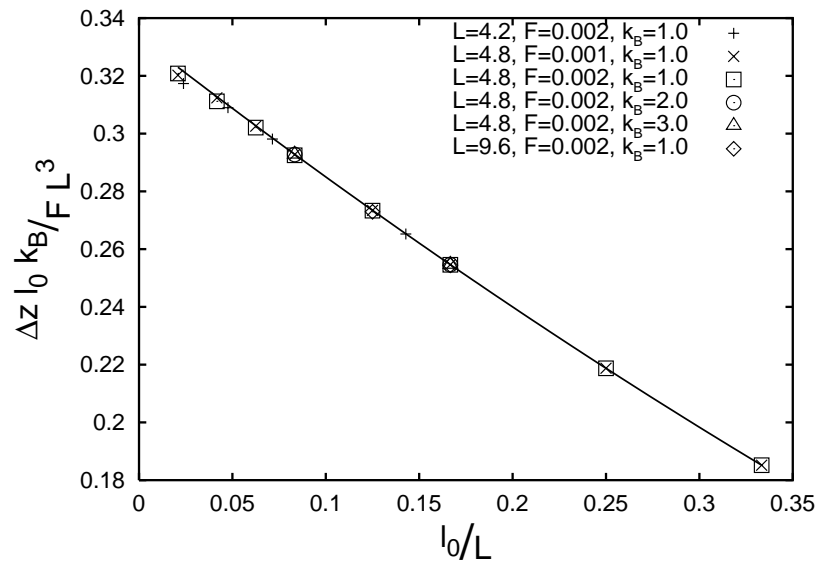


Figure 3.2: The scaled results for small deformation regime including the analytic formula (full line), too.

Fig. 3.2 presents scaled results of simulations varying the different properties of the fibers and shows agreement with the analytical formula. We recovered the classical continuum mechanics beam relationship between the deviation  $\Delta z$  and  $L^3$ :

$$\Delta z = \frac{FL^3}{EI}. \quad (3.3)$$

By analogy one can define

$$EI = \frac{3}{\left(1 - \frac{l_0}{L}\right) \left(1 - \frac{1}{2} \frac{l_0}{L}\right)} \quad (3.4)$$

in the case of the modeled fibers.

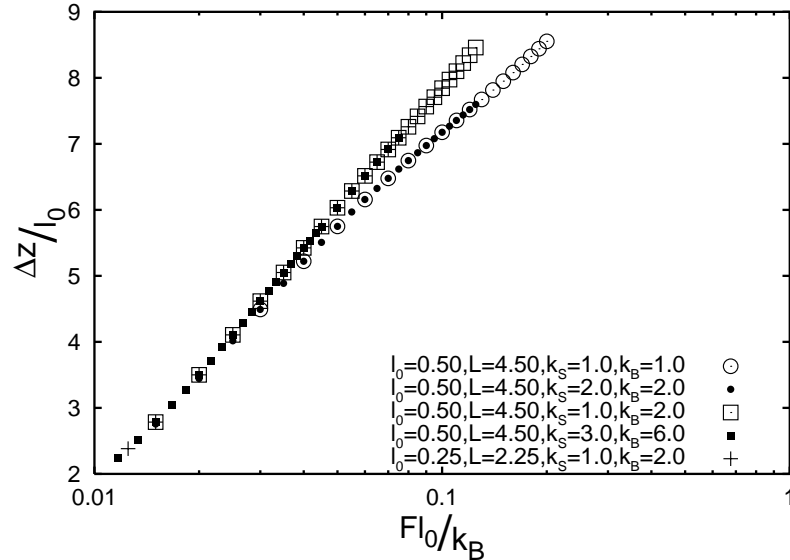


Figure 3.3: Bending-test results for large deformations of single fibers.

## 3.2 Large deformation regime

For large deformations the simulation results are compared with finite element simulations for a beam. Fig. 3.3 presents the simulated displacement which depends on the ratio between  $k_S$  and  $k_B$  (only in the large deformation regime). A linear dependence of the displacement on the logarithm of the applied force was detected in a certain range and a linear dependence on  $\frac{L}{l_0}$ , too. These results can be summarized with the following dimensionless expression:

$$\frac{\Delta z}{l_0} = \alpha \left( \frac{k_S}{k_B}, l_0 \right) \frac{L}{l_0} + \beta \left( \frac{k_S}{k_B} \right) \ln \frac{Fl_0}{k_B}. \quad (3.5)$$

In a certain range for the finite element simulations the same linear dependences were detected.

Based on these results we can conclude that in simulations we have to deal with fibers, which look like classical beams.

# 4

## Small deformation of component fibers

Firstly tangles with small volume-fractions have been studied. In this regime only small forces are present in the system and the component fibers are not bent or they are in small deformation regime. Two simulation methods are proposed.

### 4.1 Relaxation method

In the first approach a relaxation technique was employed: random tangles of different volume-fractions in a constant sized cell were produced and relaxed using the quasi-static algorithm presented above. Using this method the volume-fraction of tangles are changed with the volume of fibers i.e. with the number of component fibers.

Fig. 4.1 and fig. 4.2 presents the obtained results for the connectivity and the pressure respectively, for different values of stiffness coefficients and discretization length ( $k_S = 1.0$ ,  $k_B = 1.0$ ,  $k_I = 4.0$ ,  $l_0 = 0.5$ ). Connectivity transition is observed for fibers with shorter length than the size of the cell i.e. shorter than 5: both the number of links and the pressure are zero below critical threshold values. These threshold values are different but decrease with increasing aspect ratios as shown in fig. 4.3.

Close beyond these threshold values classical power-laws are observed

$$\frac{N_{links}}{N_{fiber}} \propto (V_f - V_{f_l}^t)^\delta \quad (4.1)$$

$$p \propto (V_f - V_{f_p}^t)^\gamma, \quad (4.2)$$

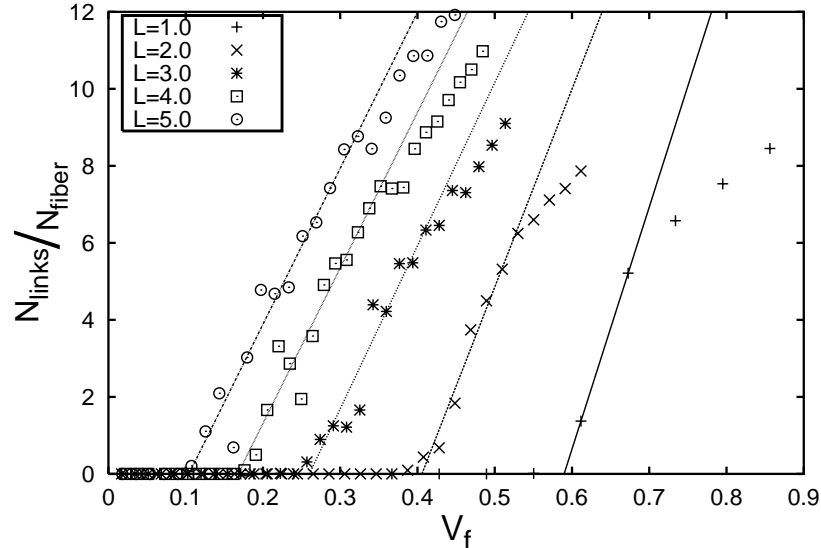


Figure 4.1: Evolution-curves for the connectivity at small deformations obtained with the relaxation method.

where  $V_{f_l}^t$  and  $V_{f_p}^t$  are the threshold values for number of links and pressure respectively, depending on the aspect ratio of fibers  $\left(\frac{L}{r_{eff}}\right)$ . The exponents found in fig. 4.1 and fig. 4.2 are  $\delta = 1$  for the connectivity and  $\gamma = 1.5$  for the pressure.

It has to be mentioned that the presented results have no statistical character since only one simulation for each curve was performed.

Using fibers longer than the size of the simulation cell, this phenomenon will not be detected. This is in agreement with our expectations since restricted boundary conditions were used. The fibers are bent from the start, so they impose pressure.

## 4.2 Compression method

The other way of simulation study of entangled materials is performing compression tests. With this method the volume-fractions are changed, by decreasing the volume of the simulation cell. Using tangles with small initial volume-fractions same curves can be obtained like with the relaxation study. This equivalence between the methods is valid only for final size of the simulation cell still larger than the length of fibers.

Fig. 4.4 and fig. 4.5 presents evolution curves for connectivity of fibers and pressure respectively, for different values of the  $k_B$ , obtained with the compression method.

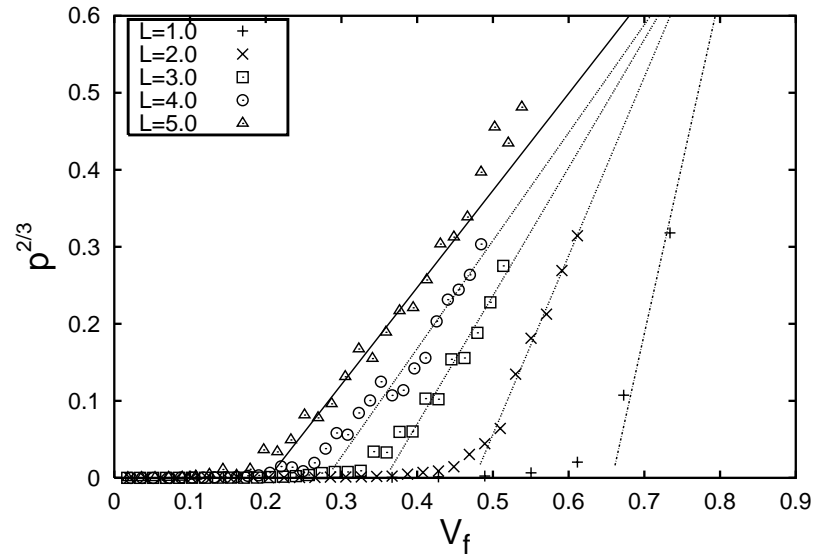


Figure 4.2: Evolution curves for pressure at small deformation of component fibers.

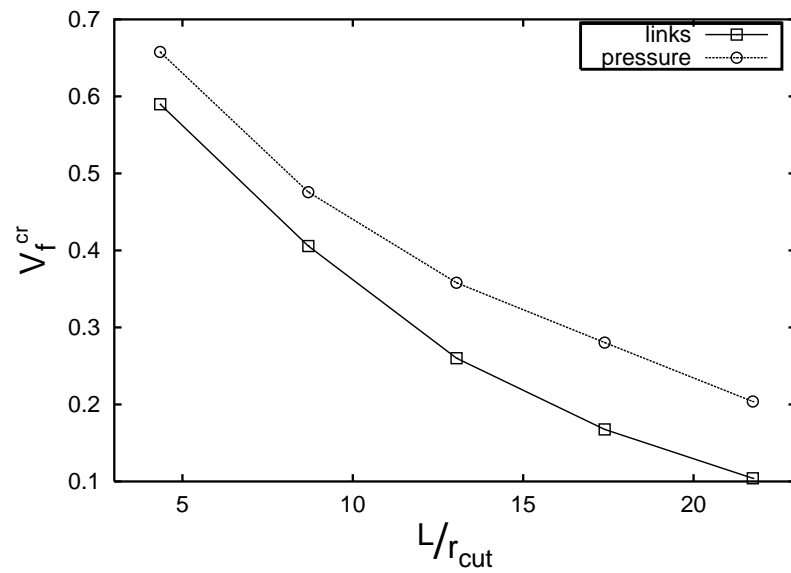


Figure 4.3: The dependence of the threshold volume-fraction on the aspect ratio of fibers.

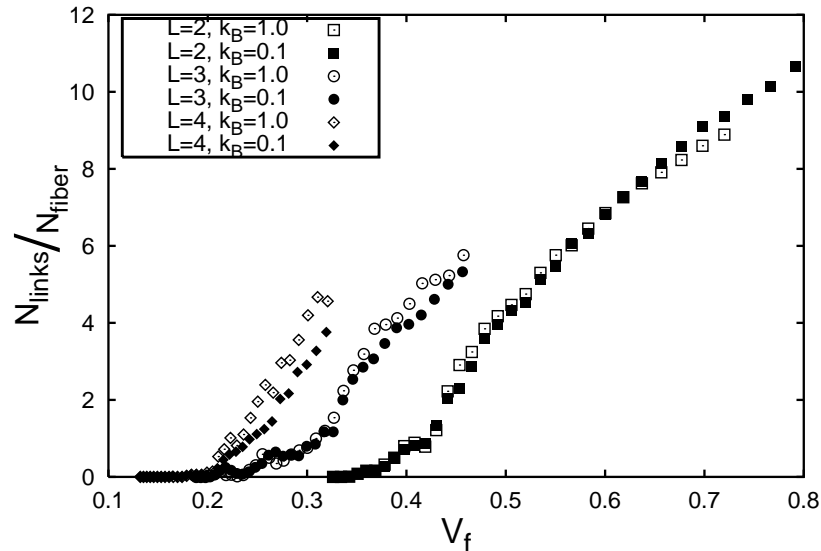


Figure 4.4: Evolution curves for the number of links per fiber, obtained with the compression method for different bending stiffnesses.

As we expected, critical volume-fractions are not depending on flexible properties of fibers. Without contact between fibers (above the threshold volume-fraction) no stretching and bending of fibers are present. On these mechanisms depends only the behavior of the system after the transition. As one can see in the graph this dependence also become important only for longer fibers and only for pressure. In addition, close beyond the connectivity threshold the fibers are in the small deformation regime with cubic dependence of its deformation on its length. They can be found in the regime described by Baudequin et al. [3].

Fig. 4.6 presents energetic aspects of the compression process. At the beginning, close to transition the compression energy is stored in interaction energy, which is greater than the other energy types. At volume fractions where bending of fibers are present the stretching and bending energies become greater than the interaction one.

We can conclude that a three-dimensional connectivity transition was found for hard-core, flexible fiber systems. This phenomenon can be linked to the three dimensional percolation, too. This model should be used to describe the electrical conductivity of entangled materials.

In order to investigate the influence of the fiber flexibility on the behavior of semi-flexible networks, tangles with higher initial volume-fractions have to be studied.

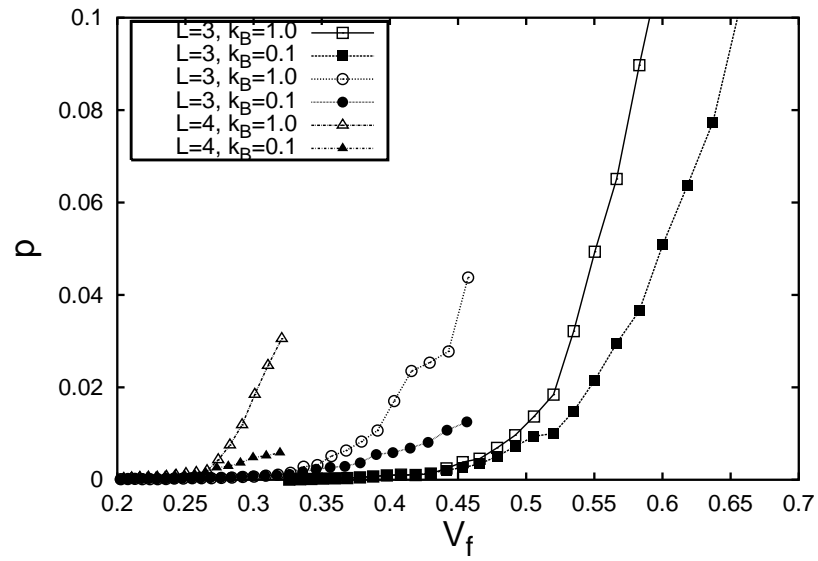


Figure 4.5: Evolution of pressure, obtained with the compression method for different bending stiffnesses.

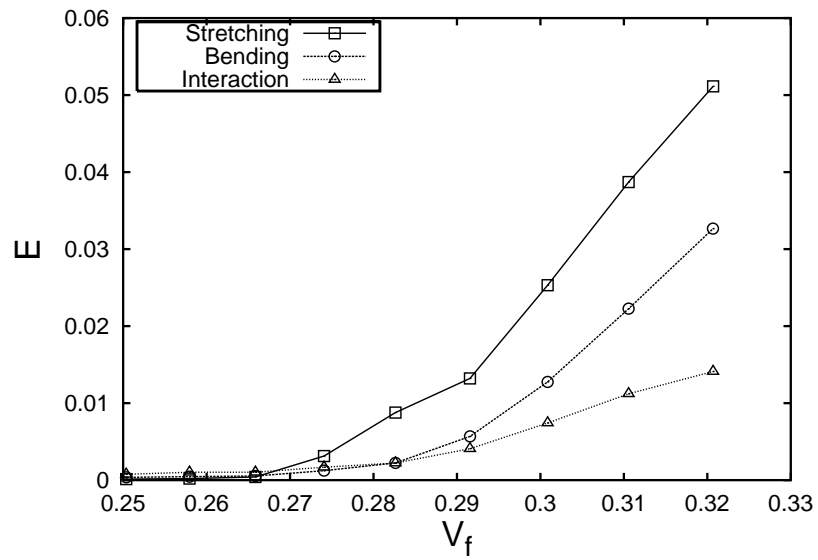


Figure 4.6: Energetic aspects for a compression process of a tangle with length  $L = 4$  of component fibers.

# 5

## Large deformations of component fibers

In order to obtain high compressibility the compression process is started with high initial volume-fractions. In this simulations the fibers can be found in the high deformation regime described above.

### 5.1 Evolution curves

Fig. 5.1 presents the evolution of the number of links for different tangles. A linear dependence on the volume-fraction can also be detected with another slope value similar with the case of small-deformed component fibers. The evolution of the links can be described as

$$\frac{N_{links}}{N_{fiber}} = \mu (V_f - V_f^*), \quad (5.1)$$

where  $\mu$  depends on aspect ratio of fibers and weakly on the  $\frac{k_S}{k_B}$  ratio.

Fig. 5.2 presents the evolution of pressure with a power-law dependence on the volume-fraction:

$$\sigma = \nu (V_f - V_f^*)^\delta. \quad (5.2)$$

On logarithmic representation different curves with same slope are obtained, so the value of  $\delta = \frac{7}{2}$  is not depending on the aspect ratio of component fibers and on flexibility parameters. The  $\nu$  parameter is also not depending on the ratio  $\frac{k_S}{k_B}$ . It depends only on aspect ratios of component fibers.

Fig. 5.3 presents the evolution of different types of energies through a compression process of a tangle composed of fibers with initial length  $L = 4$ . As one can see in

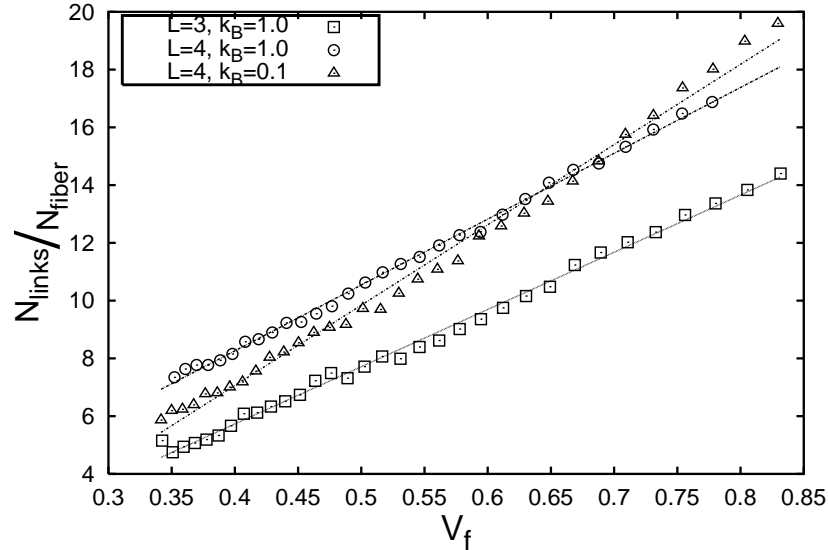


Figure 5.1: The simulation curves obtained for the compression in high deformation regime for the evolution of connectivity.

graph, all of the energies have contribution to the total energy of the system. The stretching and bending energies are evolving together. These energies are linked because the bending of a fiber imposes a contraction of its segments too.

## 5.2 Finite size effects

On presented results the effect of imposed boundary conditions can be detected. In fig. 5.4 and fig. 5.5 are presented the connectivity and the pressure evolution respectively, for two compression tests with same tangles of different initial volume-fractions. For same volume-fractions the difference between two curves consists only in the difference between the volumes of simulation cells, so in boundary conditions. As one can see in graphs, only the connectivity is affected by an underestimation of its value. The evolution of pressure is the same for both cases.

This link underestimation is responsible for slope-changing of the number of links per fiber for small deformation regime presented in the previous section on fig. 4.1 too.

In order to eliminate this boundary effect on the connectivity, the link-detection volume has to be changed. Choosing smaller detection cell inside of the simulation field this effect can be reduced.

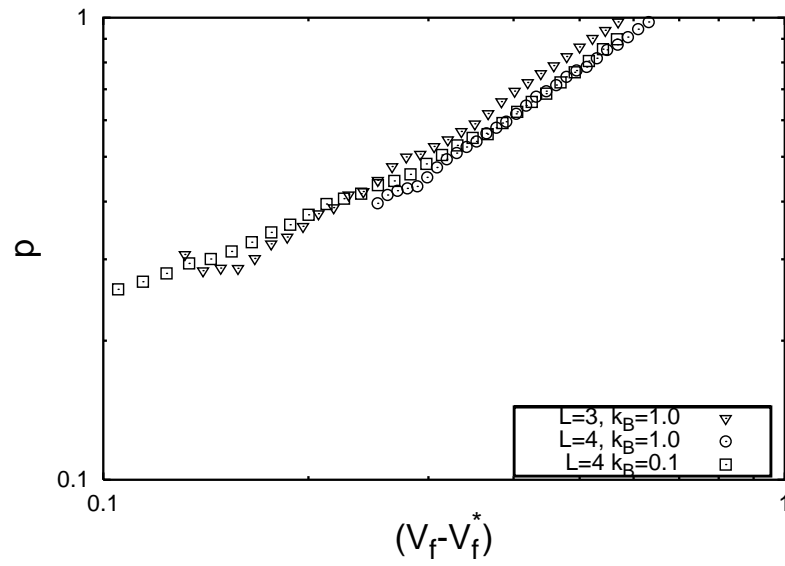


Figure 5.2: The simulation curves obtained for the compression in high deformation regime for the evolution of the pressure.

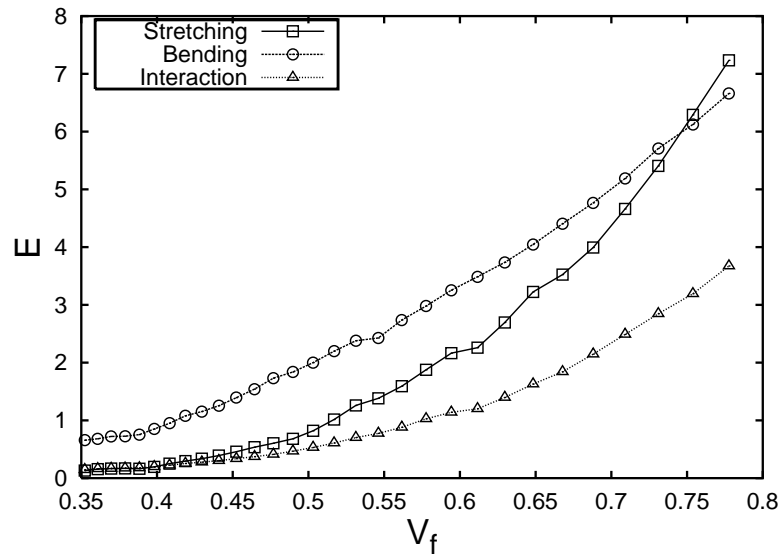


Figure 5.3: The evolution curves of different energy types for compression of a tangle in high deformation regime.

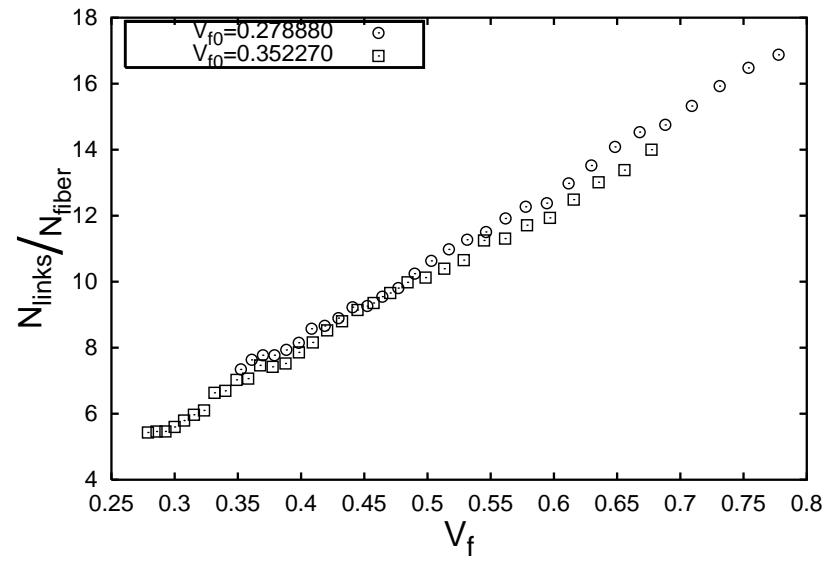


Figure 5.4: The underestimation of links caused by imposed boundary conditions.

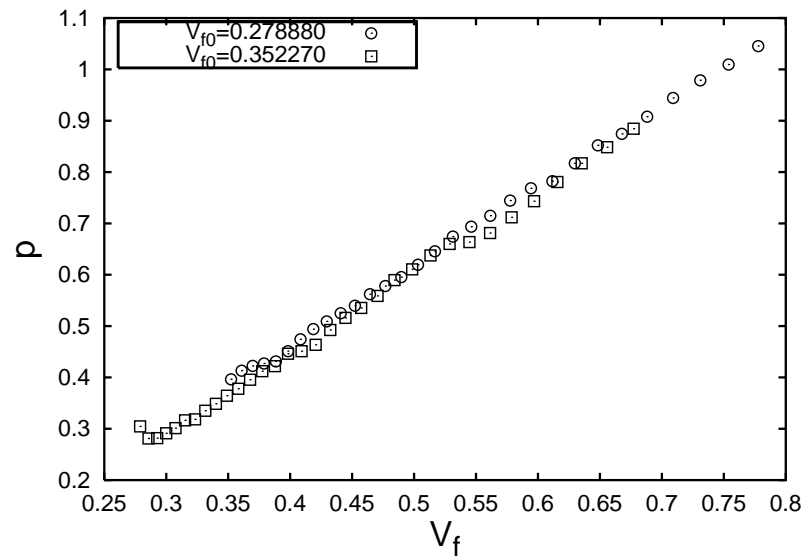


Figure 5.5: Evolution curves showing no influence of boundaries on the pressure.

# 6

## Conclusions and perspectives

Three-dimensional connectivity transition was detected for hard-core, flexible sticks system, which can be linked to three-dimensional percolation of tangles. This connectivity of fibers can be an important quantity linked to the measurable electrical conductivity of entangled materials. The transition threshold is not depending on the flexible properties of the fibers. The dependence on these properties become important only above the threshold volume-fraction and is significant only for the pressure. The behavior of the system close beyond transition can be described using the theoretical model proposed by Baudequin et al [3].

At high compression limit the fibers are in the high deformation regime and this theory cannot be applied. On one hand, the connectivity has only a weak dependence on the flexible properties of fibers in this regime, too. On the other hand the evolution of pressure shows a strong dependence on the flexibility parameters.

Looking at this observations one can conclude that the connectivity should be a pure geometrical characteristic quantity of tangles and the pressure characterize the microscopic physical processes in entangled materials. With this differences between this quantities can be explained the existence of two different but correlated transition thresholds, one for connectivity and one for pressures.

Looking at energy diagrams one can see that close to the connectivity transitions an increasing of interaction energy is present followed by the increasing of the flexibility energies. This is in agreement with our expectations that in tangles with non-connected fibers stretching or bending cannot be present. Firstly connections between fibers have to be created and after this the compression energy should be stored in flexible energy types. These observations are in agreement with the fact that

a smaller transition threshold is detected for connectivity than in case of the pressure.

In order to obtain statistical results more simulations are needed with different initial configurations. Another perspective is to reduce the effect of the boundaries on the connectivity of fibers. This problem can be solved by connectivity calculation only in a smaller volume included in the simulation cell, which will be chosen not to be in contact with the boundaries.

These simulations can be repeated using fibers with non-straight equilibrium shape. In this way one could investigate other interesting properties of the entangled materials for example the stress-strain curves for pulling on one or more fibers from tangles.

# Bibliography

- [1] I. Balberg, N. Binenbaum, N. Wagner, Phys. Rev. Lett. **52**, 1465 (1984)
- [2] Z. Néda, R. Florian, Y. Brechet, Phys. Rev. E **59**, 3717 (1999)
- [3] M. Baudequin, G. Ryschenkow, S. Roux, Eur. Phys. J. B **12**, 157 (1999)
- [4] M. Taya, W. J. Kim, K. Ono, Mechanics of Materials **28**, 53 (1998)
- [5] Peter N. Britton, Arthur J. Sampson, C. F. Elliott, Jr., H. W. Graben, W. E. Gettys, Textile Res. J **53**, 363 (1983)
- [6] I. L. Menezes-Sobrinho, Phys. Rev. E **65**, 011502 (2001)
- [7] B. Alberts, D. Bray, J. Lewis, M. Raff, K. Roberts, J. D. Watson, *Molecular Biology of the Cell* (Garland, New York, 1994); E. Frey, K. Kroy, J. Wilhelm, E. Sackmann, cond-mat/9707021 (1998)
- [8] O. Kratky, G. Porod, Rec. Trav. Chim. **68**, 1106 (1949)
- [9] F. Carmona, F. Barreau, R. Canet, P. Delhaes, J. Phys. Lett. **41**, 534 (1980)
- [10] V. Favier, R. Dendievel, G. Canova, JY. Cavaille, P. Gilormini, Acta Mater **45**, 1557 (1997)
- [11] M. P. Allen, D. J. Tildesley, *Computer simulation of liquids*, Clarendon Press, Oxford (England) (1987)
- [12] B. Hinner, M. Tempel, E. Sackmann, K. Kroy, E. Frey, Phys. Rev. Lett. **81**, 2614 (1998)
- [13] Warren. C. Young, *Roark's Formulas for Stress and Strain*, Sixth Edition, Mc. Graw-Hill, Inc., New York